(Received 11 March 2025, Accepted 22 October 2025, Scheduled 11 November 2025)

Parameter Enhancement of Vivaldi Slot 1×2 Array MIMO Antenna Using AMC

Ameet M. Mehta[1, 2, *], Shankar B. Deosarkar[1], Anil B. Nandgaonkar[1], and Avinash R. Vaidya[2]

[1] *Department of Electronics and Telecommunication Engineering*
Dr. Babasaheb Ambedkar Technological University, Lonere 402103, India
[2] *Department of Electronics and Telecommunication Engineering*
Pillai College of Engineering, New Panvel 410206, India

ABSTRACT: A wide band, high gain 1×2 array Vivaldi shaped slot Substrate Integrated Waveguide (SIW) Multiple Input Multiple Output (MIMO) antenna with square shaped periodic Artificial Magnetic Conductor (AMC) placed beneath the antenna for applications in X band is presented. A two-port MIMO antenna backed by AMC patches is designed and realized for enhanced gain and bandwidth. The single antenna 1×2 array has electrical dimensions of $1.57\lambda_r \times 1.13\lambda_r \times 0.027\lambda_r$. The designed antenna structure has bandwidth of 1.39 GHz (8.79 GHz–10.18 GHz) with a percentage bandwidth of 14.65% and gain of 11.67 dBi. The edge to edge distance between the MIMO antenna elements is 5 mm ($\lambda_r/4$). The periodic AMC patches improve vital MIMO antenna performance metrics like isolation, Envelope Correlation Coefficient (ECC), Diversity Gain (DG), Channel Capacity Loss (CCL), and radiation pattern. The unit cell analysis of periodic square AMC patch and a polynomial regression model to find the best goodness of fit for Gain-Bandwidth product versus square AMC patch size is studied. Antenna gain variation seen over the complete bandwidth is $<$ 1 dBi which makes it a flat gain response antenna. The proposed high-gain, wide-band 1×2 Vivaldi-slot SIW MIMO antenna with AMC is suitable for X-band radar, point-to-point high-throughput wireless links, and compact platform communication systems requiring robust diversity performance.

1. INTRODUCTION

Slot antennas are simple in design and provide ease in connection with other systems and circuits. However, the primary drawback of this antenna design is bidirectional radiation pattern which limits its scope of applications. Several variations in designs are reviewed to convert bidirectional radiation pattern to unidirectional one. One such method is the placement of cavities or reflectors at $\lambda/4$ periphery around a slot antenna [1, 2]. Using such an approach can make the design bulky, and moreover it provides only moderate gain. Implementing Electromagnetic Band Gap (EBG) structures beneath a slot antenna is another technique [3], but it degrades the radiation pattern and reduces gain-bandwidth product.

Substrate Integrated Waveguides (SIWs) around the periphery of a slot antenna are studied [4–6]. By placing SIW cavities around the periphery of antenna leads to low profile and directional antennas. Such antennas use Grounded Coplanar Waveguide (GCPW) feeding mechanism which simplifies the design and ensures uniform gain across the entire bandwidth [7].

Multiple Input Multiple Output (MIMO) antenna has always fascinated many researchers. Several variations in the design and configuration of MIMO antennas for various applications have been proposed. MIMO antennas show greater channel capacity if the antenna elements are arranged properly at the receiver and transmitter [8]. MIMO antennas are generally used in system for increasing data transmission rate and reducing multipath fading effects [9, 10]. It is important that designed MIMO antenna should take care of many performance metrics which include low Envelope Correlation Coefficient (ECC), high isolation (S_{12}), considerable values of Diversity Gain (DG), and Channel Capacity Loss (CCL).

For any antenna system, a key parameter is Gain-Bandwidth product. It is important to maintain the Gain-Bandwidth product optimal so that antenna can be effectively implemented in a communication system. There are numerous periodic structures which can enhance the antenna parameters as studied in [11–14]. Artificial Magnetic Conductors (AMC) are periodic structures which have in phase reflection coefficient within certain frequency range and offers high impedance. These periodic structures improve vital antenna parameters and the isolation between MIMO antenna elements.

Recent SIW-based MIMO developments demonstrate that Half-Mode SIW (HMSIW) and Quarter-Mode SIW (QMSIW) cavity structures can further improve isolation and bandwidth while reducing antenna size. For instance, an optimized compact HMSIW cavity-backed MIMO design with enhanced bandwidth is reported [15], and a QMSIW cavity-backed self-diplexing antenna with tunable resonant frequency using CSRR slots is presented in [16]. These advancements could be adapted in future designs to realize multi-port Vivaldi MIMO antennas with improved mode confinement and reduced mutual coupling.

In this paper, a 1×2 array Vivaldi shaped slot MIMO antenna integrated with SIW cavity is studied. This antenna structure is designed on a Rogers 5880 RT/Duroid substrate with dielectric

* Corresponding author: Ameet Mukund Mehta (amehta.dbatu@gmail.com).

constant of 2.2 and loss tangent of 0.0009. The single antenna array structure has electrical dimensions of $1.57\lambda_r \times 1.13\lambda_r \times 0.027\lambda_r$. The 1×2 array MIMO antenna with square periodic AMC patches placed beneath the antenna structure is designed to give wideband and high gain response, and the measured bandwidth is 1.39 GHz (8.79 GHz–10.18 GHz) while the maximum measured gain is 11.67 dBi. The gain variation over the complete band is < 1 dBi which makes the antenna a flat gain response antenna. The vital MIMO antenna parameters are well in control. Measured value of Envelope Correlation Coefficient (ECC) is < 0.001, Diversity Gain (DG) between 9.993 to 9.998, and average Chanel Capacity Loss (CCL) 0.263 b/s/Hz. With the placement of periodic AMC patches, the radiation pattern, isolation, and Front-to-Back ratio improve.

2. ANTENNA GEOMETRY AND ANALYSIS

2.1. Design of the Slot

The tapered curve or Vivaldi shaped curve slot is created beneath the substrate. The slot is designed using Equation (1).

$$m = pe^{rn} \tag{1}$$

where 'm' is vertical position, 'p' the scaling factor, 'r' the exponential growth, and 'n' horizontal position.

The geometry of the tapered shaped curve slots is as seen in Fig. 1. The variations in the values of 'p' and 'n' generate two Vivaldi shaped curve slots. The curves are placed as mirror images back-to-back to get the desired tapered shaped curve.

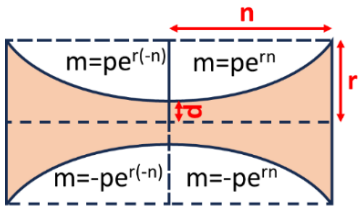

FIGURE 1. Antenna slot geometry.

The Vivaldi slot geometry is generated using an exponential taper profile in Equation (2), which provides a gradual impedance transition from the feed to the radiating aperture. This taper ensures broadband performance and stable phase characteristics.

The slot contour is defined by the exponential relation:

$$y(x) = \pm Ae^{Bx}, \quad 0 \le x \le L_{slot} \tag{2}$$

where A is the initial half-width of the slot at the feed point, B the exponential flare rate, and L_{slot} the total slot length along the x-axis.

The constants A and B are determined using the boundary conditions as seen in Equation (3):

$$B = \frac{1}{L_{slot}} \ln\left(\frac{y_L}{y_0}\right), \quad A = y_0 \tag{3}$$

where y_0 and y_L represent the half-widths of the slot at the throat and aperture, respectively. The exponential law governs the rate of field expansion and directly affects impedance and radiation behavior as shown in Equation (3).

For the proposed design, parameters are optimized at $L_{slot} = 14.1\,\text{mm}$, $y_0 = 0.362\,\text{mm}$, and $y_L = 4.05\,\text{mm}$, giving $B = 0.171\,\text{mm}^{-1}$. These values offer an effective compromise between impedance bandwidth and aperture efficiency. The slot length is approximately $0.7\lambda_r$, where $\lambda_r = \lambda_o/\sqrt{\varepsilon_r}$ is the guided wavelength at the first resonance frequency.

2.2. Design of the Antenna Structure

The simulated antenna is designed with following dimensions $0.72\lambda_r \times 1.07\lambda_r \times 0.027\lambda_r$ where the value of λ_r is calculated at first resonance frequency. The slot has a perimeter of $1.40\lambda_r$. Slot antennas have bidirectional radiation pattern. To achieve unidirectional radiation pattern, Substrate Integrated Waveguide (SIW) cavity is created along the periphery. This cavity is created by incorporating via holes which create a short in the antenna and ground plane. This shorting results in unidirectional radiation pattern.

The SIW via holes have diameter 'd' of 1 mm, and 's' is 1.6 mm which is thedistance between two via holes. These dimensions are selected to maintain following ratios as given in Equation (4) [17]. Maintaining these ratios becomes essential for minimizing leakage current in the antenna structure.

$$\frac{d}{\lambda_r} \le 0.1 \quad \text{and} \quad \frac{d}{s} \ge 0.5 \tag{4}$$

The antenna geometry seen in Fig. 2 is designed using a Rogers 5880 RT/Duroid substrate with dielectric constant (ε) of 2.2 and loss tangent of 0.0009.

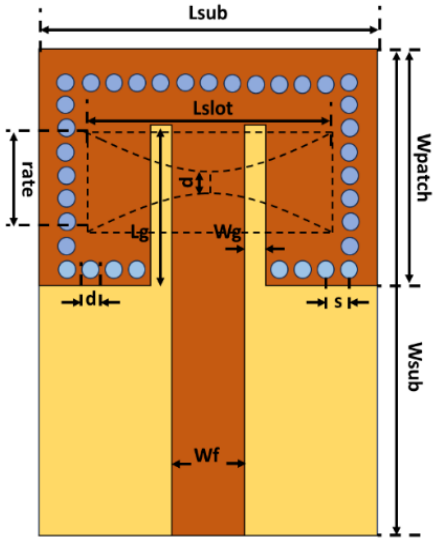

FIGURE 2. Simulated antenna structure.

The design is simulated using High Frequency Structure Simulator (HFSS) 19.1 software.

2.3. Parametric Analysis of the Antenna

The parametric analysis is done by varying the values of length 'L_{slot}', rate 'r', and scaling factor 'p'. The slot length is varied

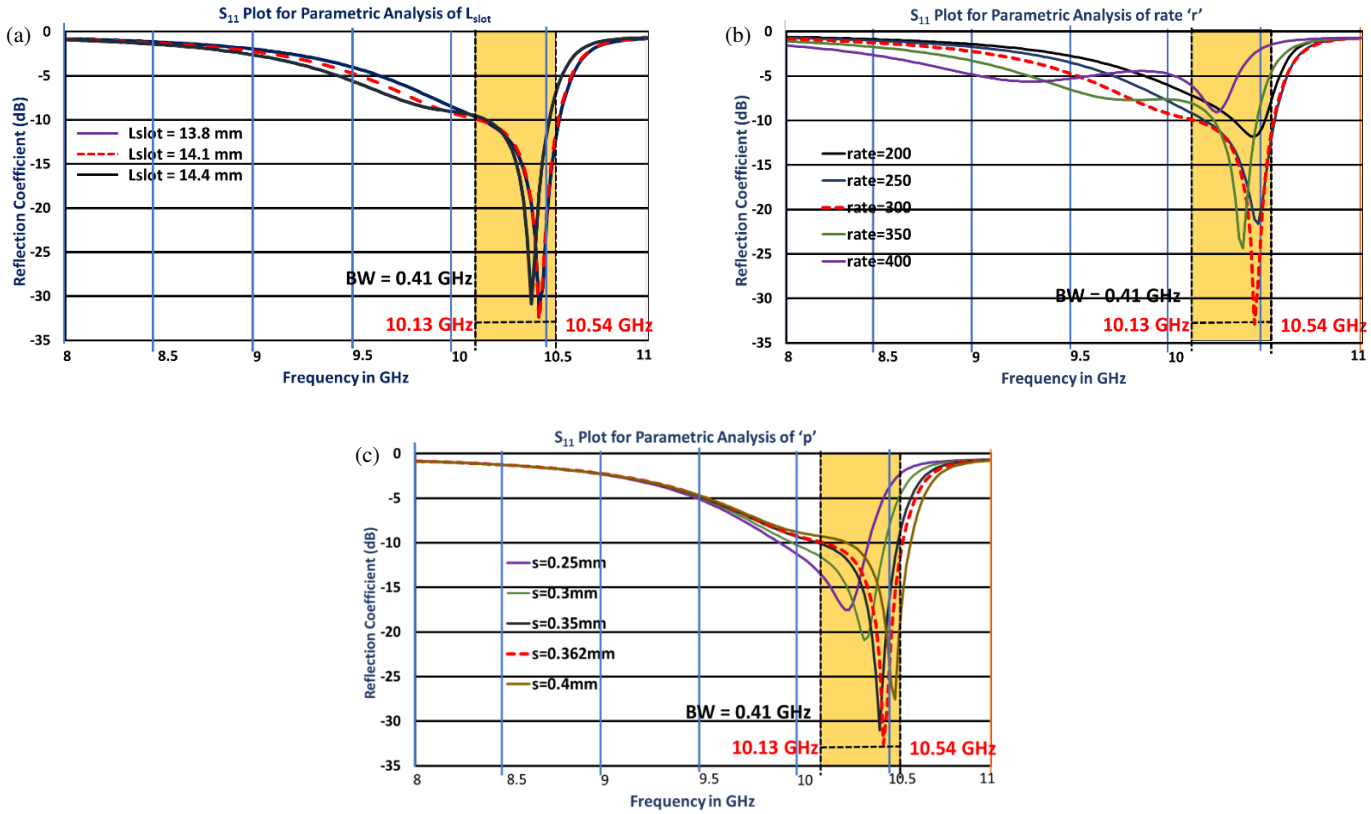

FIGURE 3. S_{11} plot for parametric analysis of (a) slot length L_{slot}, (b) rate 'r', (c) small length 'p'.

in steps of 0.3 mm from 13.8 mm to 14.4 mm, and the parameter rate 'r' is varied in steps of 50 mm from 200 to 400. The scaling factor 'p' is varied in steps of 0.05 mm from 0.25 mm to 0.4 mm. The S_{11} plot shown in Fig. 3(a) shows variations in resonating frequency and bandwidth for parametric analysis for length 'L_{slot}'. While the S_{11} plot shown in Fig. 3(b) shows variations in resonating frequency and bandwidth for parametric analysis for rate 'r', and Fig. 3(c) shows the S_{11} plot for variation in value of 'p'. The optimised values of 'L_{slot}', 'r', and 'p' selected from S_{11} plot are 14.1 mm, 300, and 0.362 mm, respectively. Table 1 shows the antenna geometry designed values.

TABLE 1. Antenna geometry designed values. All values in mm except 'r'. Rate 'r' is a number.

Sr. No	Parameter	Value	Sr No	Parameter	Value
1	L_{sub}	20.9	7	L_g	11
2	W_{sub}	31	8	W_g	1.2
3	H_{sub}	0.787	9	W_{patch}	19
4	L_{slot}	14.1	10	d	1
5	r	300	11	s	1.6
6	W_f	2.4	12	p	0.362

From the plots as shown in Fig. 3, it becomes obvious that the maximum bandwidth achieved after parametric analysis is 0.41 GHz (10.13 GHz–10.54 GHz) with centre frequency of 10.40 GHz. The structure also offers a gain of 6.03 dBi.

3. DESIGN OF 1 × 2 MIMO ANTENNA

MIMO antennas are intended to be used in applications where high gain and wide band responses are required. The tapered curve or Vivaldi curve slot antenna is particularly used for applications which demand wide band and high gain responses. Some of the applications where Vivaldi antenna plays an important role are radar and communication system.

3.1. Design of 1 × 2 Antenna Array

The 1 × 2 array antenna is seen in Fig. 4. Designed array is for specific feed lines to ensure proper impedance match. The array is fed to ensure coherent radiation utilizing 100 Ω, 70.7 Ω (Quarter-wave transformer), and 50 Ω microstrip feed line. The fed method adopted ensures the proper impedance matching between antenna array elements and feed network. This antenna structure promotes optimal power transfer and minimizes reflections. The single array structure has design dimensions of $1.57\lambda_r \times 1.13\lambda_r \times 0.027\lambda_r$ and provides bandwidth of 0.16 GHz and improved gain of 8.32 dBi as seen in Fig. 5.

3.2. Design of 1 × 2 Array MIMO Antenna

The 1 × 2 array MIMO antenna is as seen in Fig. 6. In this configuration the two 1 × 2 antenna array elements are placed op-

TABLE 2. 1 × 2 MIMO antenna performance metrics.

Sr. No	Parameter	Value
1	Envelope Correlation Coefficient (ECC)	0.001
2	Diversity Gain (DG)	9.995–10 dB
3	Total Active Reflection Coefficient (TARC)	−16.74 dB at resonance
4	Mean Effective Gain (MEG)	−3.09 dB
5	Channel Capacity Loss (CCL)	0.038 bps/Hz at resonance

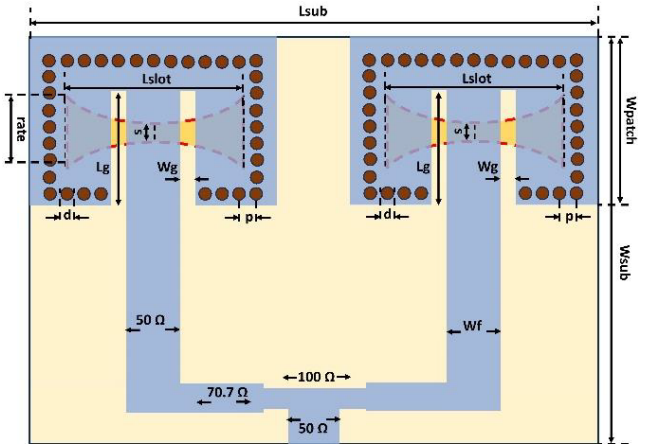

FIGURE 4. Geometry of 1 × 2 antenna array.

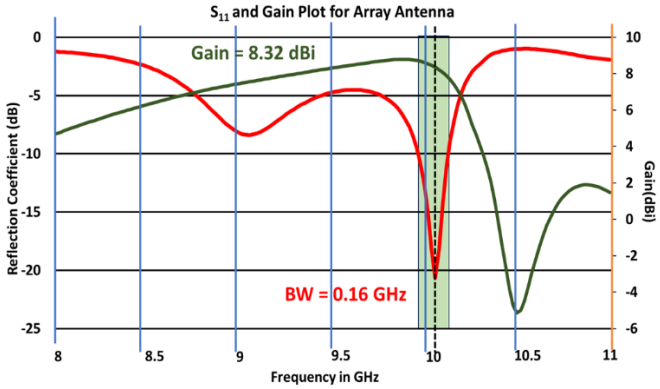

FIGURE 5. Antenna 1 × 2 array S_{11} and gain plot.

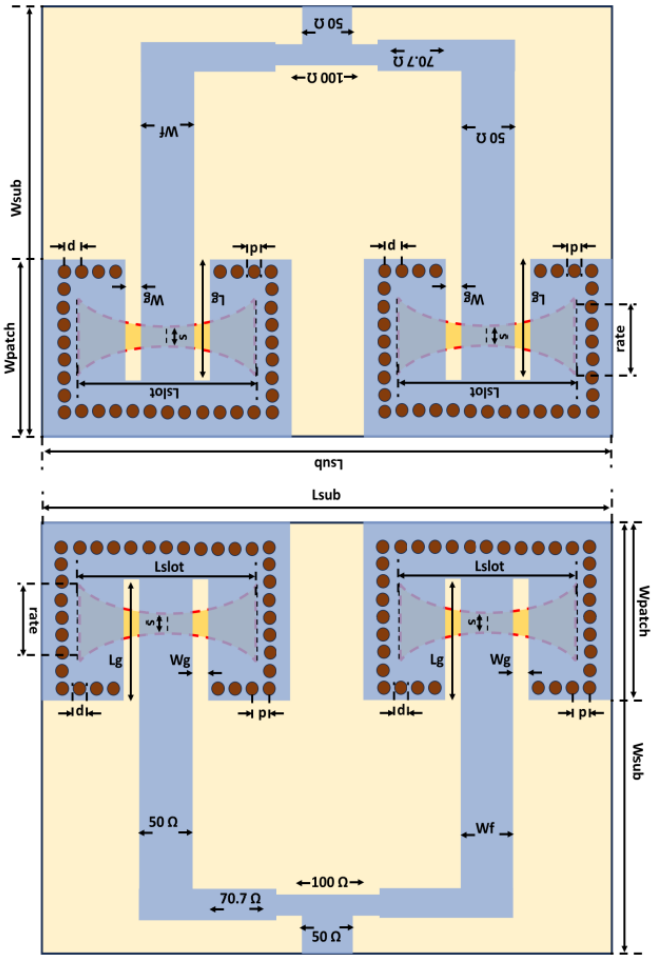

FIGURE 6. 1 × 2 array MIMO antenna geometry.

posite to each other at a distance less than $\lambda_r/4$. $\lambda_0 = 30$ mm, $\lambda_r = \lambda_0/\sqrt{2.2} \approx 20.23$ mm, i.e., $\lambda_r/4 \approx 5.06$ mm. Fig. 7 shows S_{11} plot for MIMO antenna. The MIMO antenna resonates at 10.15 GHz and S_{11} value of −23.62 dB. The MIMO antenna has bandwidth of 0.18 GHz (10.06 GHz–10.24 GHz). The isolation S_{12} value at resonance is −20.29 dB. The isolation value is < -20 dB over the complete band. The gain at resonance frequency is 8.93 dBi. Thus, with MIMO configuration there is improvement observed in gain as well as bandwidth.

The MIMO antenna performance metrics are in the range of standard prescribed values. Table 2 shows the simulated MIMO antenna performance metrics.

The MIMO antenna performance metrics are in the range of standard prescribed values. Table 2 shows the simulated MIMO antenna performance metrics.

4. DESIGN OF AMC PATCHES

The unit cell analysis of single unit cell of AMC patches was performed using full-wave Floquet port analysis in HFSS 19.1 software. Unit cell analysis is required to study the behaviour and resonance characteristics of AMC patches. The variation in patch size and periodicity of the patches is studied to understand their effects on various antenna parameters.

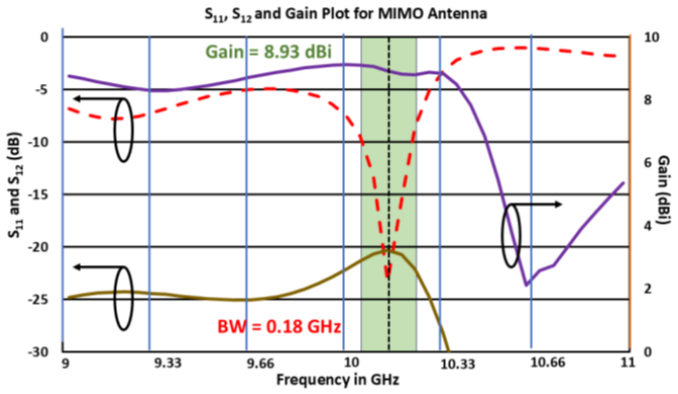

FIGURE 7. S_{11}, S_{12}, and gain plot for 1×2 array MIMO.

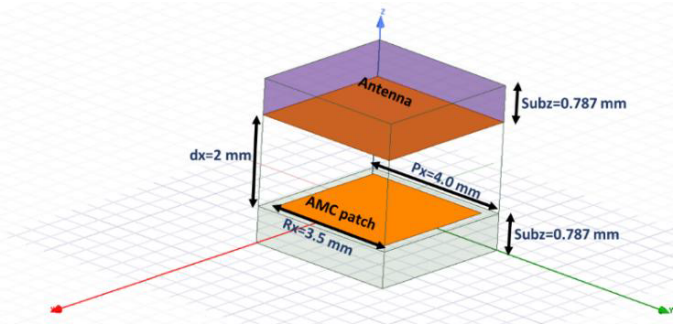

FIGURE 8. Unit cell simulated structure.

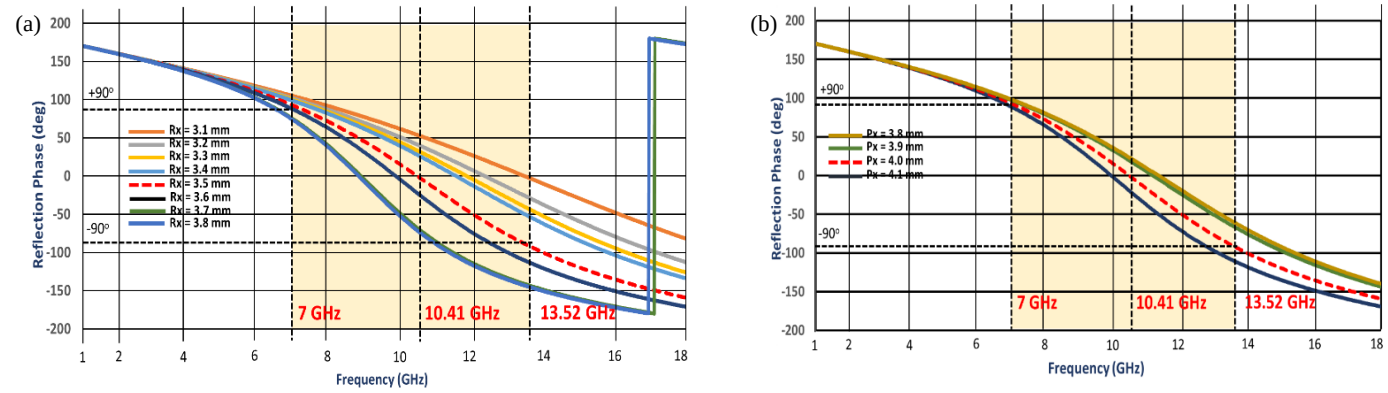

FIGURE 9. Parametric analysis of unit cell. (a) Patch size Rx. (b) Periodicity Px.

As seen in Fig. 8, the unit cell of the AMC is placed below the antenna structure. This arrangement reveals how the periodic AMC patches interact with the antenna element. A 2 mm distance is kept between the antenna and the AMC. The spacing between the two is very crucial to understanding the interaction between the antenna and AMC surface. The placement of AMC patches enhances critical parameters like gain, bandwidth, and efficiency of the antenna. It also improves impedance matching thus improving the radiation characteristics of the antenna.

The unit cell configuration of the patches with its periodicity directly impacts the resonating frequency and the reflection phase. AMC patches exhibit 0° reflection phase with a corresponding ± 90 bandwidth. For efficient performance in the desired frequency range, these characteristics are essential

Parametric analysis as seen in Fig. 9 is by varying the patch size 'Rx'. The patch size is varied in steps of 0.1 mm from 3.1 mm to 3.8 mm. The reflection phase becomes 00 at 10.41 GHz for patch size $Rx = 3.5$ mm. The corresponding bandwidth spans from 7 GHz to 13.52 GHz. With the increase in patch size, shift in resonant frequency is observed towards lower frequencies, and bandwidth is also reduced.

The periodicity of the AMC unit cell is analysed by varying the value of 'Px'. The value of Px is incremented by 0.1 mm from 3.8 mm to 4.1 mm. The reflection phase becomes 00 at 10.41 GHz for $Px = 4$ mm. The corresponding bandwidth observed is from 7 GHz to 13.52 GHz. With increase in value of Px, both the bandwidth and resonating frequency get expanded.

Thus, from above observations the unit cell patch size 'Rx' selected is 3.5 mm while the periodicity 'Px' selected is 4 mm. This configuration is selected as the resonating frequency is 10.41 GHz which is like antenna resonating frequency.

5. 1×2 MIMO ANTENNA WITH AMC PATCHES

The simulated structure of 1×2 array MIMO antenna with AMC patches placed beneath is as seen in Fig. 10(a). The side view configuration of the same antenna is as seen in Fig. 10(b). The AMC patches are placed beneath at 2 mm from the Vivaldi shaped slot antenna. The placement of AMC patches beneath the 1×2 array Vivaldi shaped slot antenna improves antenna performance parameters.

The S_{11}, S_{12}, and gain plot for 1×2 array MIMO antenna with square AMC patches beneath is as seen in Fig. 11. Placing AMC patches beneath it significantly improves antenna parameters like bandwidth and gain. The bandwidth achieved with this configuration is 1.41 GHz (8.77 to 10.18 GHz), and gain improves to 11.92 dBi. The isolation between the antenna elements also improves and is nearly -30 dB over the complete band. Applications requiring high directional performance and signal strength can use these crucial improvements.

TABLE 3. Gain-bandwidth product variation with respect to the patch size.

Patch Size (mm)	Reso1 $`f'_{01}$ (GHz)	S_{11} Value (dB)	Gain at Reso1 (dBi)	Reso2 $`f'_{02}$ (GHz)	S_{11} Value (dB)	Gain at Reso2 (dBi)	Freq. f_1 (GHz)	Gain at f_1 (dBi)	Freq. f_2 (GHz)	Gain at f_2 (dBi)	Band -width f_2–f_1 (GHz)	Peak Gain in Band (dBi)	Avg. Gain $`Ax'$ (dBi)	Avg. Gain $`A'$ in Linear Scale	Gain -Bandwidth Product (GHz)
2.5	9.25	−25.34	10.41	10.10	−29.61	10.48	8.94	10.00	10.26	10.00	1.32	10.71	10.32	10.76465	**14.20**
3	9.20	−25.60	10.81	10.00	−36.49	10.43	8.84	10.39	10.21	9.75	1.37	10.93	10.46	11.144	**15.23**
3.5	**9.15**	**−17.51**	**11.82**	**9.95**	**−26.19**	**11.73**	**8.77**	**11.59**	**10.18**	**11.26**	**1.41**	**11.92**	**11.66**	**14.66898**	**20.68**
4	9.22	−14.39	11.48	9.90	−22.35	11.00	8.79	11.08	10.14	10.23	1.35	11.51	11.06	12.76439	**17.23**
4.5	9.21	−14.24	11.08	9.90	−15.58	11.23	8.86	10.60	10.09	10.65	1.23	11.47	11.00	12.6066	**15.50**

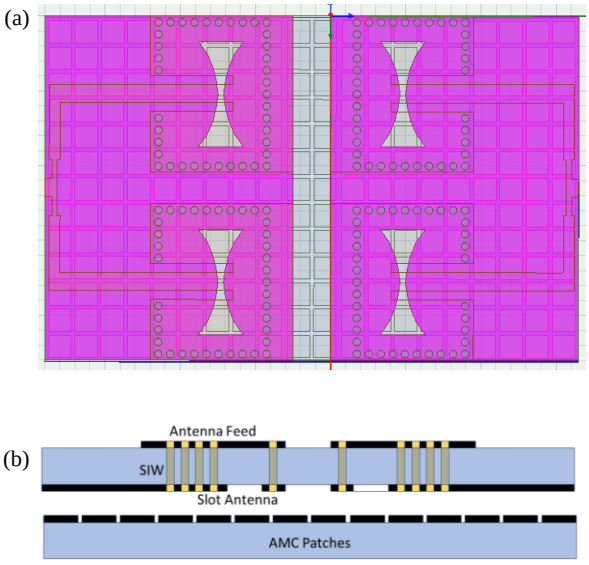

FIGURE 10. Simulated MIMO-AMC structure. (a) Top view. (b) Side view.

6. POLYNOMIAL REGRESSION MODEL

6.1. Gain-bandwidth Product Calculation

The important performance metric for an antenna design is Gain-Bandwidth product. The design of the antenna should be optimized to get maximum gain bandwidth product. Different sets of frequencies and gain simulated for varying AMC patch size while the distance dx is maintained constant ($dx = 2$ mm) are shown in Table 3. The AMC patch size is varied from 2 mm to 4.5 mm in steps of 0.5 mm.

The Gain-Bandwidth product is calculated in GHz by converting gain in dBi to linear gain using Equation (5).

$$\text{Gain in linear scale } A = 10^{\left(\frac{Ax}{10}\right)} \tag{5}$$

where Ax is the gain in dBi.

The Gain-Bandwidth product calculated from Table 3 is by multiplying the averages of all the gain taken at different frequencies with the bandwidth. The gain-bandwidth product is an important performance metric for an wide band and high gain response antenna. The placement of AMC patches beneath the antenna helps in improving and enhancing antenna parameters.

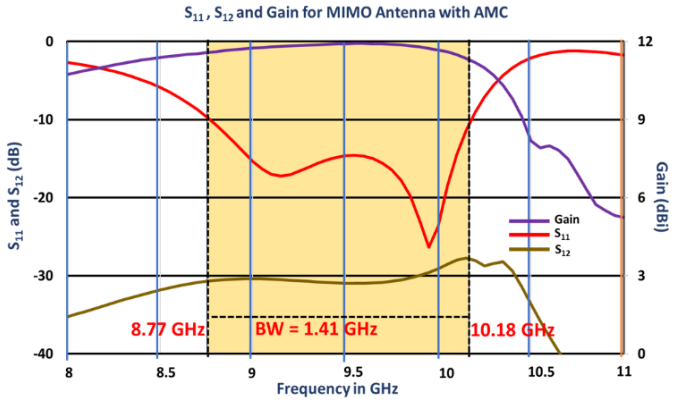

FIGURE 11. S_{11}, S_{12} and gain plot for 1×2 array MIMO antenna with AMC patches beneath.

A graph for Table 3 is plotted in excel, where the x-axis represents the AMC patch size in mm while y-axis represents gain-bandwidth product in GHz. Polynomial trendlines of order $n = 2$ to $n = 5$ was plotted to model the relationship between the AMC patch size on x-axis and the gain-bandwidth product on y-axis.

From the graph in Fig. 12, polynomial trend-lines of orders $n = 2$ to $n = 5$ were plotted to model the relationship between patch size (x) and Gain-Bandwidth product (y).

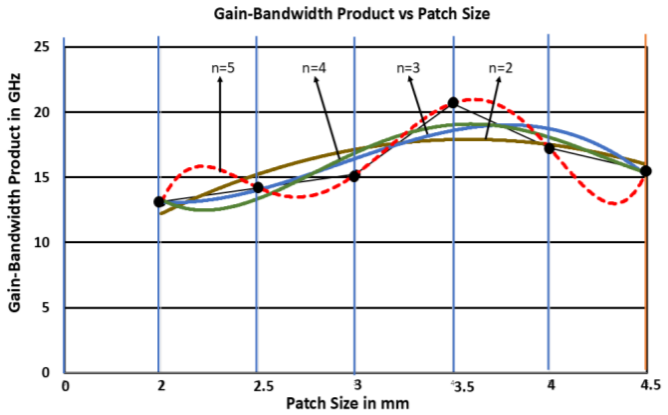

FIGURE 12. Polynomial fitted curve for varying patch size vs gain-bandwidth product.

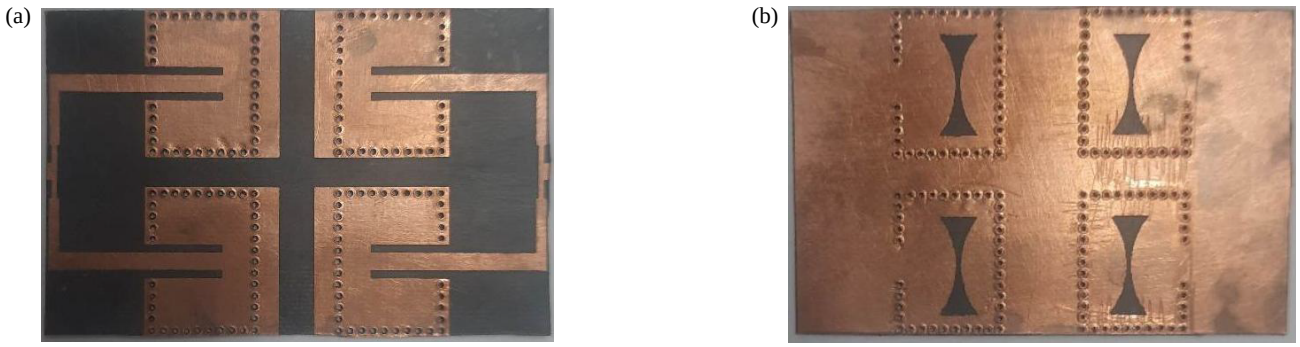

FIGURE 13. Fabricated antenna structure. (a) Top view. (b) Bottom view.

FIGURE 14. Experimental setup for MIMO antenna with AMC patches.

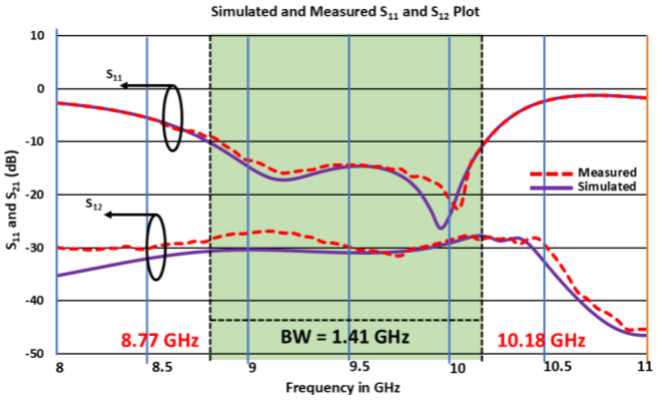

FIGURE 15. Measured and simulated S_{11} and S_{12} for MIMO antenna.

An R^2 value of 1 indicates a perfect fit, meaning that the polynomial curve of order 5 accurately models the relationship between patch size (x) and Gain-Bandwidth Product (y).

The polynomial trend-line equation for $n = 5$ is:

$$y = 0.3476x^5 - 5.95455x^4 + 37.6956x^3 - 108.61x^2 + 141.59x - 51.924 \text{ for } R^2 = 1 \quad (6)$$

where y represents the Gain-Bandwidth Product, and x denotes the patch size as depicted in Equation (6).

According to Table 3, the optimal Gain-Bandwidth Product is achieved with a patch size of 3.5 mm. At $Rx = 3.5$ mm, the bandwidth is 1.41 GHz; the average gain over the band is 11.66 dBi; and the Gain-Bandwidth Product is 20.683 GHz. This confirms that the optimal patch size yields the best performance in terms of both gain and bandwidth, leading to an improved overall antenna efficiency.

7. SIMULATED AND MEASURED RESULTS

A tapered curve (Vivaldi) shaped slot 1×2 array MIMO antenna design is presented in this section along with the simulation using HFSS 19.1 software, and fabricated on a Rogers 5880 RT/Duroid substrate with a dielectric constant of 2.2 and a tan δ of 0.0009. The fabricated structure is seen in Figs. 13(a) and (b). The antenna's performance was evaluated through S_{11} and S_{12} measurements, which were conducted using a Keysight N9928A Vector Network Analyzer at Dr. Babasaheb Ambedkar Technological University, Lonere. Additionally, the radiation pattern was measured in an anechoic chamber at BITS Pilani, Goa, with a standard horn antenna used for reference. These measurements provided both reflection and transmission characteristics, as well as insight into the antenna's directional performance, allowing for a comprehensive assessment of its MIMO capabilities.

The measured S_{11} and S_{12} values of tapered curve (Vivaldi) slot 1×2 array MIMO antenna show close match with the simulated results. The experimental setup is shown in Fig. 14. The comparison between the simulated and measured results confirms the accuracy in designing of the antenna. The measured bandwidth is 1.39 GHz (8.79 GHz–10.18 GHz). The resonance is obtained at 9.15 GHz and 10.05 GHz as seen in Fig. 15. The S_{12} value, which indicates the isolation between the two antenna elements, was measured to be less than -25 dB, slightly higher than the simulated isolation of less than -30 dB. Despite this, the antenna demonstrates a bandwidth of 1.39 GHz with isolation greater than -25 dB, confirming its effective performance in MIMO applications. There is a slight shift in resonance observed at high frequency due to fabrication tolerances. The simulated and measured gain plots for 1×2 array MIMO antenna are shown in Fig. 16. The maximum measured gain of 11.67 dBi is observed at 9.5 GHz. Despite minute differences between the simulated and measured gains, the overall gain response remains relatively flat throughout operating frequency range of the antenna.

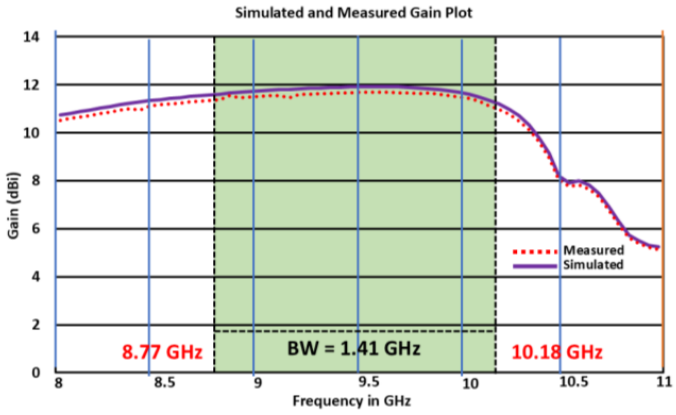

FIGURE 16. Gain plot for MIMO measured and simulated.

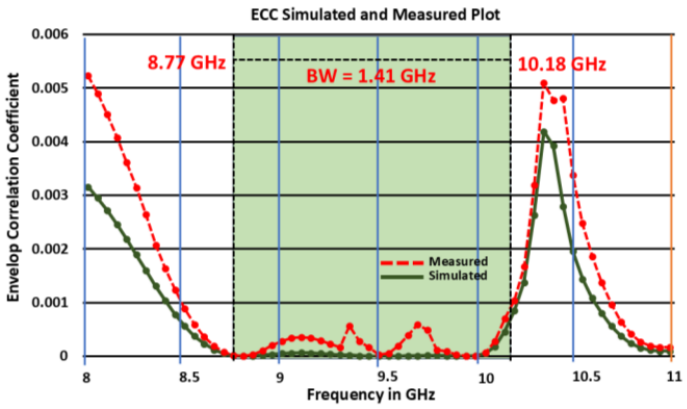

FIGURE 17. ECC plot for MIMO measured and simulated.

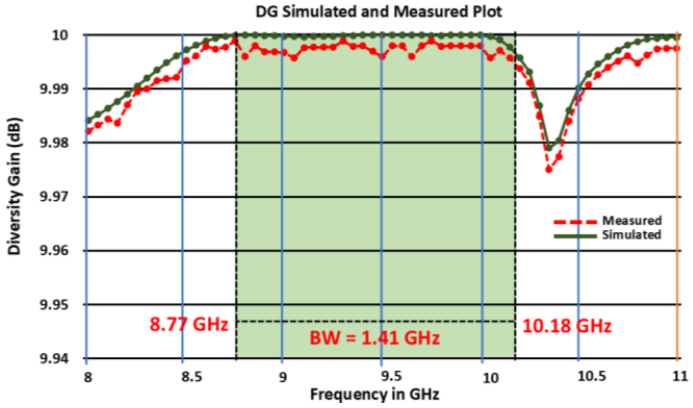

FIGURE 18. DG plot for MIMO measured and simulated.

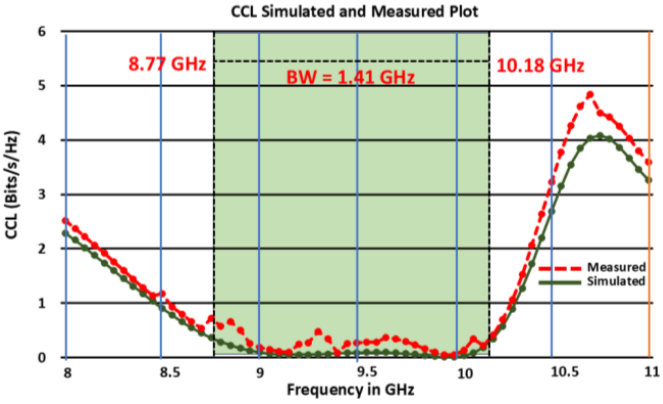

FIGURE 19. CCL plot for MIMO measured and simulated.

A small frequency shift ($\sim$ 100 MHz) is observed between simulated and measured S_{11} curves. This deviation arises from fabrication and connector tolerances; however, the measured bandwidth (8.79–10.18 GHz) and isolation ($\leq$ -25 dB) validate the simulation trends.

Measured and simulated Envelope Correlation Coefficients (ECCs) remain below 0.001 over the complete bandwidth of 1.41 GHz as seen in Fig. 17. The optimal value of ECC should be below 0.5 for enhancing diversity and reducing mutual coupling.

The measured value of Diversity Gain (DG) is between 9.993 dB and 9.998 dB as seen in Fig. 18. The simulated DG value is between 9.9975 dB and 10 dB for the complete band of 1.41 GHz. The value of DG is well within the limits required for MIMO antenna diversity performance.

The simulated average Channel Capacity Loss (CCL) over the complete simulated bandwidth of 1.41 GHz is 0.1052 b/s/Hz, while the average CCL value measured is slightly higher 0.263 b/s/Hz across the same bandwidth as seen in Fig. 19.

Figure 21 shows E-plane and H-plane radiation patterns, measured and simulated at 9.95 GHz. The Sidelobe Level (SLL) measured is -16 dB indicating efficient radiation. The cross polarizations in E-plane and H-plane are well within the acceptable levels. E-plane cross polarization is below -22 dB, while H-plane cross polarization is below -29 dB. The front-to-back ratio is 24.78 dB.

All the required MIMO antenna performance metrics designed are well within the standard values required for efficient working of MIMO antenna. Thus, placing AMC patches below the 1×2 array Vivaldi shaped slot MIMO antenna improves performance and maximizes throughput in real world communication environment.

Figure 20 shows measured and simulated E-plane and H-plane radiation patterns at 9.15 GHz. The Sidelobe Level (SLL) measured is -16 dB indicating efficient radiation. The cross polarizations in E-plane and H-plane are well within the acceptable levels. E-plane cross polarization is below -25 dB, while H-plane cross polarization is below -24 dB. The front-to-back ratio is 30.59.

Figure 22 shows the 2-D radiation efficiency vs frequency for the proposed 1×2 MIMO antenna with and without AMC. The AMC-backed configuration demonstrates a higher and flatter radiation efficiency across the operating band ($\approx$ 89–91%) than the baseline ($\approx$ 78–80%). This improvement is consistent with the measured gain increase (from $\approx$ 8.9 dBi to $\approx$ 11.7 dBi) and the AMC's suppression of surface-wave losses and back-radiation.

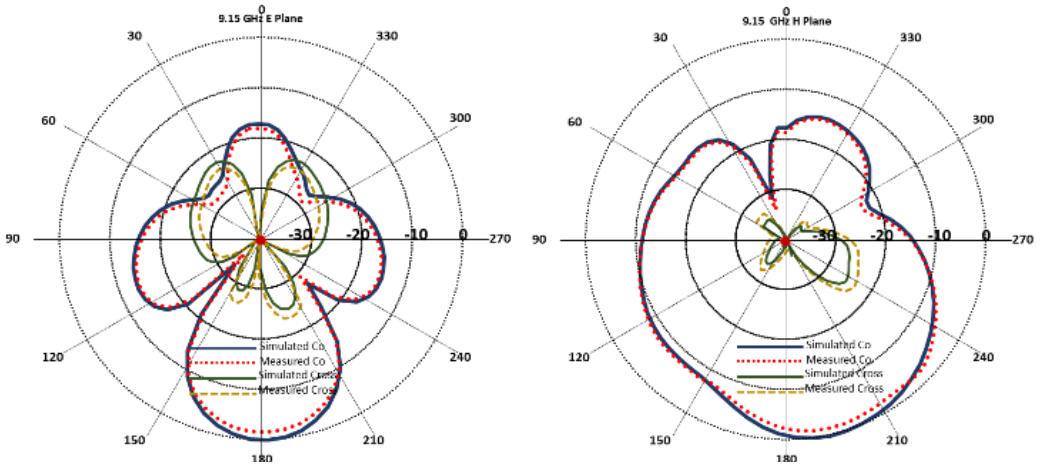

FIGURE 20. Radiation pattern measured and simulated in E-plane and H-plane at 9.15 GHz.

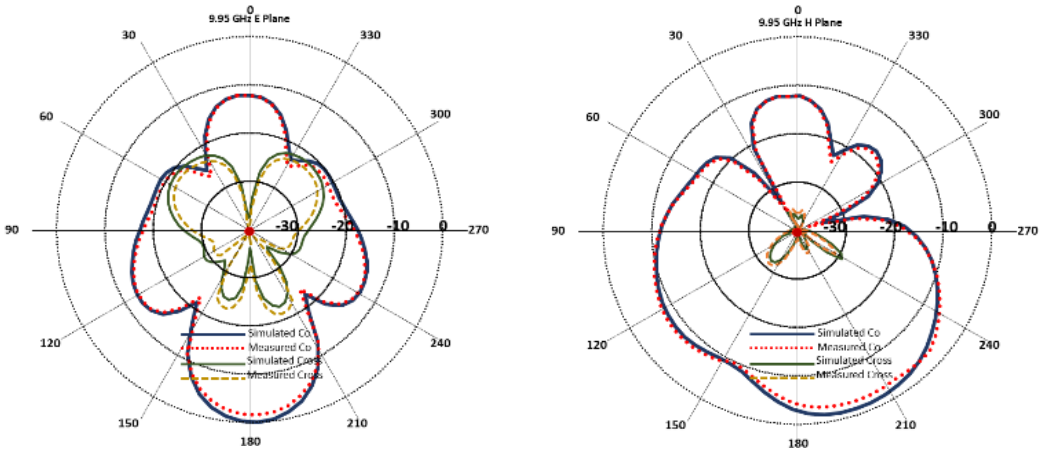

FIGURE 21. Measured and simulated radiation patterns in E-plane and H-plane at 9.95 GHz.

TABLE 4. Comparison of the proposed work with the existing literature.

Ref. No	Antenna Dimension	$S_{11} < -10$ dB Bandwidth GHz	% Bandwidth	S_{12} Isolation (dB)	Gain (dBi)	ECC
[18]	$0.87\lambda \times 0.87\lambda \times 0.19\lambda$	3.0–4.1 GHz 1.1 GHz	31.00%	$>$ 25 dB	7.1 dBi	0.010
[19]	$0.73\lambda \times 0.73\lambda \times 0.0280\lambda$	6.0–11.5 GHz 5.5 GHz	62.85%	20 dB	3.5–7 dBi	$<$ 0.1
[20]	$0.83\lambda \times 0.83\lambda \times 0.024\lambda$	4.0–13.5 GHz 9.5 GHz	108.57%	$\geq$ 23.4 dB	1.8–6.7 dBi	$\leq$ 0.002
[21]	$2.21\lambda \times 1.32\lambda$	5.9 GHz	6.9%	$>$ 24 dB	9.6 dBi	0.002
[22]	$0.91\lambda \times 0.91\lambda \times 0.045\lambda$	7.2–9.1 GHz 1.9 GHz	15.4%	$>$ 20 dB	5.2 dBi	$<$ 0.005
[23]	$1.63\lambda \times 0.58\lambda \times 0.023\lambda$	2.33–14.83 GHz 12.5 GHz	145.6%	23 dB	5.89 dBi	0.002
PW	$1.57\lambda \times 2.26\lambda \times 0.027\lambda$	8.79–10.18 GHz 1.39 GHz	14.88%	$>$ 25 dB	11.67 dBi	$<$ 0.001

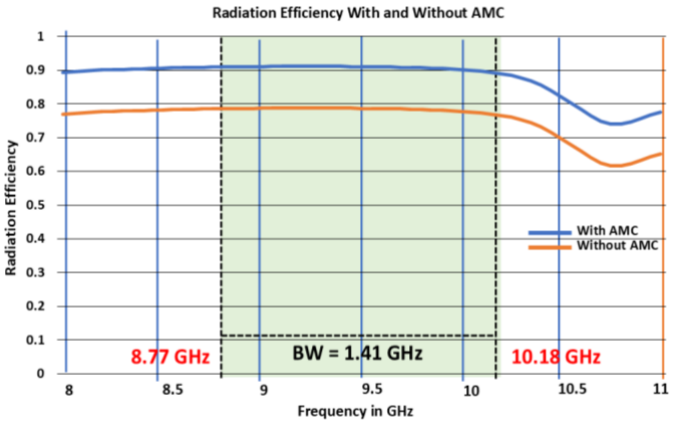

FIGURE 22. Simulated radiation efficiency with and without AMC.

8. COMPARISION AND DISCUSSIONS

Table 4 shows the comparison between the proposed structure and existing literature. The 1×2 array MIMO slot antenna integrated with SIW provides high gain and wide band response. The two antenna array elements have moderate dimensions but provide excellent gain, bandwidth, isolation, and MIMO antenna performance metrics. The antenna has very low ECC < 0.001 which is better than other antennas compared in the table. The SIW integrated antenna is closely packed with the distance between two MIMO elements $< \lambda/4$ which provides better isolation than almost all other works compared in the table.

The proposed work shows improvement in Gain and ECC as compared to [18–23]. The bandwidth and percentage bandwidth of [19, 20] and [22–23] are more than proposed work, but the isolation of the proposed work is better than [19–23].

Although the antenna's aperture dimension contributes to the overall gain, the key improvement results from the AMC-backed SIW configuration that enables uniform current distribution and reduced back radiation. The regression-based AMC optimization (Equation (4)) shows that the gain-bandwidth product peaks at a specific patch size 3.5 mm, confirming that the performance enhancement arises from electromagnetic optimization rather than physical enlargement.

9. CONCLUSION

A High Gain and Wide Band 1×2 Array Vivaldi Shaped Slot with SIW integrated MIMO Antenna with AMC patches is presented and demonstrated. The use of periodic AMC patches enhances the performance of the antenna. The 1×2 MIMO antenna with periodic AMC patches has bandwidth of 0.18 GHz and gain of 8.93 dBi. The placement of periodic AMC patches beneath improves both bandwidth and gain to 1.39 GHz and 11.67 dBi. The isolation also improves and becomes > 25 dB. All the MIMO antenna performance metrics improve like ECC, DG, CCL, and radiation pattern. The F/B ratio for MIMO antenna is 30.59 dB and 24.78 dB at 9.15 GHz and 9.95 GHz, respectively. The gain variation over the complete band is < 1 dBi which makes the antenna flat gain response and suitable for MIMO communication system.

REFERENCES

[1] Verbiest, J. R. and G. A. E. Vandenbosch, "Low-cost small-size tapered slot antenna for lower band UWB applications," *Electronics Letters*, Vol. 42, No. 12, 670–671, 2006.

[2] Yoshimura, Y., "A microstripline slot antenna (short papers)," *IEEE Transactions on Microwave Theory and Techniques*, Vol. 20, No. 11, 760–762, Nov. 1972.

[3] Locker, C., T. Vaupel, and T. F. Eibert, "Radiation efficient unidirectional low-profile slot antenna elements for X-band application," *IEEE Transactions on Antennas and Propagation*, Vol. 53, No. 8, 2765–2768, Aug. 2005.

[4] Xiong, J., X. Li, and B.-Z. Wang, "A novel low-profile slot antenna with unidirectional radiation," in *The 8th European Conference on Antennas and Propagation (EuCAP 2014)*, 1443–1445, The Hague, Netherlands, 2014.

[5] Gao, X., Y. Qi, and Y.-C. Jiao, "Design of multiplate backreflector for a wideband slot antenna," *IEEE Antennas and Wireless Propagation Letters*, Vol. 12, 773–776, 2013.

[6] Mukherjee, S., A. Biswas, and K. V. Srivastava, "Broadband substrate integrated waveguide cavity-backed bow-tie slot antenna," *IEEE Antennas and Wireless Propagation Letters*, Vol. 13, 1152–1155, 2014.

[7] Mukherjee, S., A. Biswas, and K. V. Srivastava, "Substrate integrated waveguide cavity-backed dumbbell-shaped slot antenna for dual-frequency applications," *IEEE Antennas and Wireless Propagation Letters*, Vol. 14, 1314–1317, 2015.

[8] Addepalli, T. and V. R. Anitha, "A very compact and closely spaced circular shaped UWB MIMO antenna with improved isolation," *AEU — International Journal of Electronics and Communications*, Vol. 114, 153016, 2020.

[9] Sheikh, J. A., Z. Ahmad, S. A. Paraha, and G. M. Bhat, "A compact dual band MIMO antenna for WLAN applications," in *2016 IEEE Annual India Conference (INDICON)*, 1–4, Bangalore, India, 2016.

[10] Es-Saleh, A., M. Bendaoued, S. Lakrit, S. Das, and A. Faize, "Design aspects of MIMO antennas and its applications: A comprehensive review," *Results in Engineering*, Vol. 25, 103797, 2025.

[11] Fang, S., L. Zhang, Y. Guan, Z. Weng, and X. Wen, "A wideband Fabry-Perot cavity antenna with single-layer partially reflective surface," *IEEE Antennas and Wireless Propagation Letters*, Vol. 22, No. 2, 412–416, Feb. 2023.

[12] Mehta, A. M., S. B. Deosarkar, and A. B. Nandgaonkar, "Design and development of CPW-fed miniaturized MSA for improved gain, bandwidth and efficiency using PRS," *Progress In Electromagnetics Research C*, Vol. 137, 211–222, 2023.

[13] Jagtap, S., A. Chaudhari, N. Chaskar, S. Kharche, and R. K. Gupta, "A wideband microstrip array design using RIS and PRS layers," *IEEE Antennas and Wireless Propagation Letters*, Vol. 17, No. 3, 509–512, Mar. 2018.

[14] Zhou, E., Y. Cheng, F. Chen, H. Luo, and X. Li, "Low-profile high-gain wideband multi-resonance microstrip-fed slot antenna with anisotropic metasurface," *Progress In Electromagnetics Research*, Vol. 175, 91–104, 2022.

[15] Pramodini, B., D. Chaturvedi, L. Darasi, G. Rana, and A. Kumar, "Optimized compact MIMO antenna design: HMSIW-based and cavity-backed for enhanced bandwidth," *IEEE Access*, Vol. 12, 189 820–189 828, 2024.

[16] Chaturvedi, D. and A. Kumar, "A QMSIW cavity-backed self-diplexing antenna with tunable resonant frequency using CSRR slot," *IEEE Antennas and Wireless Propagation Letters*, Vol. 23, No. 1, 259–263, Jan. 2024.

[17] Xu, F. and K. Wu, "Guided-wave and leakage characteristics of substrate integrated waveguide," *IEEE Transactions on Microwave Theory and Techniques*, Vol. 53, No. 1, 66–73, Jan. 2005.

[18] Zhu, J., S. Li, S. Liao, and Q. Xue, "Wideband low-profile highly isolated MIMO antenna with artificial magnetic conductor," *IEEE Antennas and Wireless Propagation Letters*, Vol. 17, No. 3, 458–462, Mar. 2018.

[19] Sasikumar, J. and V. Koushick, "Performance analysis of complementary split ring resonator with improved four element antenna for X band wireless applications," *Progress In Electromagnetics Research M*, Vol. 130, 95–102, 2024.

[20] Li, R., H. Zhang, Y. Xu, and J. Hou, "A compact two-port Vivaldi-based MIMO antenna with high isolation for C and X bands applications," *Progress In Electromagnetics Research Letters*, Vol. 120, 95–101, 2024.

[21] Sarkar, G. A., K. M. Parvez, A. Ambika, T. Islam, S. Das, U. Mandal, and S. K. Parui, "A quad port MIMO antenna using rectangular dielectric resonator antenna array for intelligent transportation system applications," *Progress In Electromagnetics Research M*, Vol. 123, 45–52, 2024.

[22] Khan, I., K. Zhang, L. Ali, and Q. Wu, "A compact FSS-based four-port MIMO antenna for low mutual coupling," *IEEE Antennas and Wireless Propagation Letters*, Vol. 22, No. 12, 2836–2840, Dec. 2023.

[23] Saleh, S., T. Saeidi, N. Timmons, B. Alali, F. Razzaz, and A. A. Althuwayb, "Compact ultra-wide band two element vivaldi non-uniform slot MIMO antenna for body-centric applications," *Results in Engineering*, Vol. 24, 102839, 2024.